DETECTION AND CLASSIFICATION OF LIVER CANCERS USING COMPUTED TOMOGRAPHY IMAGES

G.B. SOLOMON[*#], *A.G. ABEBE*[*], *D.S. TEFERI*[**], *M.M. MENGISTE*[***]

*Department of Physics, College of Natural and Computational Sciences, Haramaya University, Haramaya, Ethiopia, [#]e-mail: binysoul@gmail.com
**Radiology Department, College of Health Sciences, Tikur Anbessa Specialized Hospital, Addis Ababa University, Addis Ababa, Ethiopia
***Department of Medicine, College of Health Science and School of Medicine, Dire Dawa University, Dire Dawa, Ethiopia

Abstract. The aim of this research was to develop an appropriate algorithm that can automatically detect and classify liver cancers. Digital image processing (DIP) provides different techniques for the segmentation and classification purposes. The sample was taken from 36 abdominal CT scans from Tikur Anbessa Specialized Hospital in DICOM stored in Addis Ababa. Semi-automatic techniques were used to segment liver images from the abdominal CT images then artificial neural network (ANN) was applied for classification of liver out of the given sample through nine texture features into 12 normal and 24 abnormal images. Then, liver tumors were segmented from the 24 abnormal liver images using the histogram-based Otsu method. The classification of liver tumors was performed by using ANN through six morphological features into 12 benign and 12 malignant. The classification results are presented in this paper using the confusion matrix, which shows 95.8 % maximum accuracy rate of tumor classification. However, the performance of the classifier could be improved by more sample images. The outcome of this work may help radiologists to identify tumors at early stages and to classify them as benign or malignant. The methodology proposed here might reduce the fatality rate of liver cancers in Ethiopia.

Key words: Digital image processing, ANN, liver cancers, CT images.

INTRODUCTION

Liver cancer is caused by uncontrolled growth of liver cells that might result in a lump of cohesive cells referred as tumor. A tumor arises from a pathologic disturbance of cell growth, characterized by excessive and abnormal proliferation of cells; it can either be solid or fluid filled [15].

There are various types of liver tumors such as benign, malignant, and metastases. A benign tumor is non-cancerous, not posing serious threat to health;

Received: February 2023;
in final form March 2023.

ROMANIAN J. BIOPHYS., Vol. 32, No. 4, P. 219–233, BUCHAREST, 2022

benign tumors are quite common and do not spread to other parts of the body. The most common types of benign tumors are hemangioma and cysts, whereas a malignant liver tumor is a primary liver cancer, which may originate from the liver and can spread to other parts of the body. The most common examples of malignant tumors are cholangio-carcinoma and hepatocellular carcinoma (HCC). A chronic liver disease, HCC is caused either by alcohol consumption of viral infection. Such infections of the liver are referred to as hepatitis, and they account for 75 % of all liver cancers [12].

Malignant tumors such as HCC, have poor prognosis, with few treatments offering long term survival. If not detected at an early stage, HCC has indeed a poor prognosis of low survival rate (with a range of 20–40 %) after surgical resection; depending on the histology and the extension of the lesions. The only treatments with a curative value are surgical resection, liver transplantation and percutaneous ablation [3].

According to the *Ethiopian Journal of Health Development* [10], Ethiopia lags far behind in addressing HCC, compared to other countries. There is no national policy framework and guideline for the management of HCC. Health professionals working in health care facilities should share the data they have to the scientific community and policy makers, for further searching solutions and informed decisions. An intensified public health strategy on health education early case detection is of critical importance. In addition concerted effort should be made to develop HCC prevention and treatment methods. However, studies conducted in Ethiopia on computer aided diagnostic (CAD) system for chronic liver diseases are limited. Hence, there is an utter need of CAD systems capable of providing an accurate and effective classification of liver tumors.

Various medical imaging modalities can be employed for the diagnosis of liver cancers such as ultrasound (US), computed tomography (CT), magnetic resonance imaging (MRI), and angiography. However, CT is preferred over those modalities because of its high accuracy, sensibility and specificity. Moreover a CT scan is quick, may be done with or without contrast agents, it produces detailed images at high resolution, it is painless, and generally safe [6]. Also CT images can give specific information about the size, shape, and location of liver tumors [2]. Hence, this work investigated the possibility of identification and classification of liver tumors by analyzing CT images.

METHODOLOGY

This research was designed to develop computer vision techniques for detection and classification of liver cancers by using image processing and neural network toolboxes from MATLAB (Natick, MA, USA). Figure 1 presents the flow diagram of the proposed methodology.

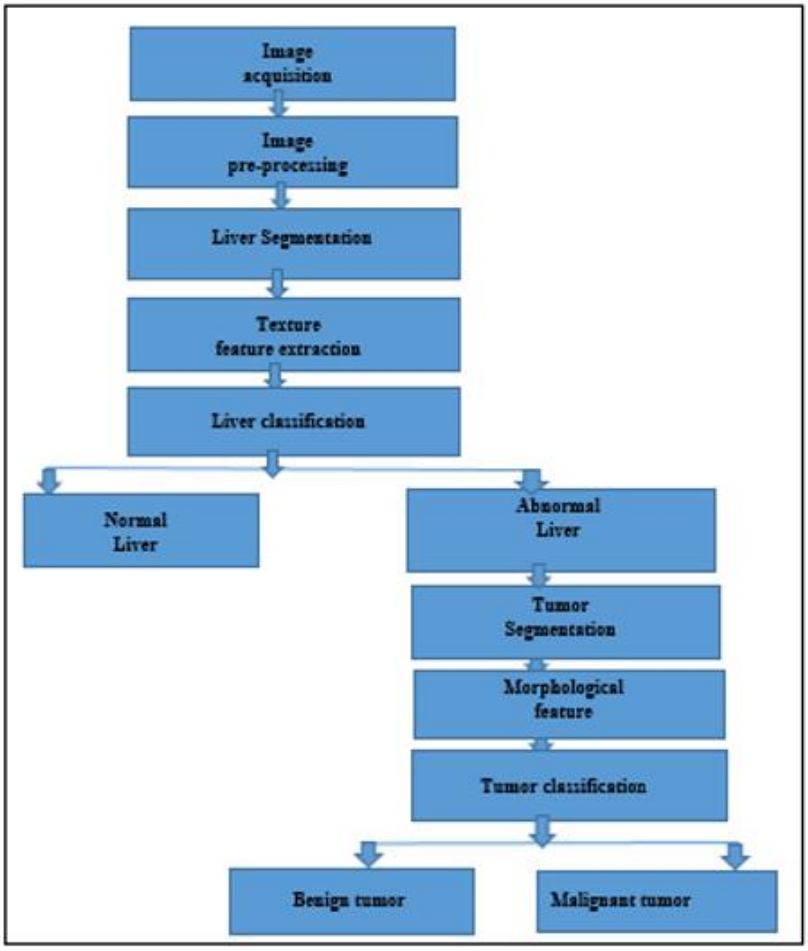

Fig. 1. The proposed methodology.

IMAGE ACQUISITION AND PREPROCESSING

The CT images were stored in digital image and communications in medicine (DICOM) format. They were collected from Black Lion Hospital based in Addis Ababa. One slice of 128 slices of images that clearly shows liver in axial view of perdiagnosed patient was taken by the help of a radiologist. Before image segmentation, an erosion technique was employed to remove unwanted background such as CT marks using the "diamond" structure element with a "radius of 2" as proposed by Sahoo *et al*. [13]. Then median filtering operation was performed to reduce the effect of impulsive noise. The median filter used a 5×5 kernel size, as recommended by Malik *et al.* [8].

LIVER SEGMENTATION

The liver is both of highly variable shape and it displays a low difference in appearance compared to the neighboring organs, such as diaphragm, the stomach, or the spleen [9]. Thus, the segmentation of the liver is a very difficult task. In this work, the segmentation liver image from abdominal CT image was performed by using semi-automatic technique. It was performed first by free hand drawing on the boundary of the liver that cut-off the non-liver region without losing pixels that belong to the region of the liver. Then, the free hand selection creates a binary mask image from the ROI (liver) with all pixel values inside the liver to 1, and all pixel values outside the ROI to 0. Lastly, the liver was delineated from other part of the CT image by green component segmentation.

TEXTURE FEATURE EXTRACTION

After segmentation of liver from abdominal CT image, nine texture features were extracted. Texture analysis is rich in visual information and is a key component in image analysis [7]. To obtain textural features, the co-occurrence matrix was calculated first. It estimates the repeated occurrence of gray level configuration as one transverses the image along a certain distance and direction [7].

An occurrence of a gray level configuration described by a matrix of relative frequencies $\mathbf{P}_{\theta,d}(i,j)$, giving how frequently two pixels with gray levels appear in the window separated by a distance d in direction θ and these matrices are symmetric, $\mathbf{p}_{\theta,d} = \mathbf{P}_{\theta,d}(i,j)$. This function determines how frequently a pixel with the intensity (gray-level) value i occur in a particular spatial relationship to a pixel with the value j to produce a gray-level co-occurrence matrix (GLCM). The pixel of interest and the pixel immediately to its right (horizontally adjacent) are the default definitions of the spatial relationship, but can be specified by other spatial relationships between the two pixels. The number of times the input image's pixel with the value i occurred in the specified spatial relationship to a pixel with value j is simply added for each element (i,j) in the final GLCM [5]. The gray-level co-occurrence matrix (GLCM) normalized by dividing each entry of the matrices by the total number of pairs as follows:

$$\mathbf{p}(i,j) = \frac{\mathbf{P}(i,j)}{n} \tag{1}$$

where, $\mathbf{p}(i,j)$ is the normalized GLCM and $\mathbf{P}(i,j)$ is the un-normalized GLCM and n is the normalization factor, which is equal to the total number of pairs. Texture features measured using GLCM derived quantities by taking the ratio of each normalized GLCM elements multiplied by a logarithmic function of mean grey-level intensity for fine to medium texture ratio ($\sigma = 0.5$ and 1.5) in enhanced liver images.

These values could be considered to represent the relative contributions made by each fine and medium texture ratio [14]. This texture ratio quantification was used because the ratio would be effectively normalized, thereby minimizing the effects of any potential variations in CT attenuation values occurring from one image to another and also reducing the effect of noise on texture quantification.

$$TR = \frac{\sum_{i,j=1}^{n} \mathbf{P}(i,j)_{\sigma=0.5} \log_2 \mathbf{P}(i,j)_{\sigma=0.5}}{\sum_{i,j=1}^{n} \mathbf{P}(i,j)_{\sigma=1.5} \log_2 \mathbf{P}(i,j)_{\sigma=1.5}} \tag{2}$$

where, *TR* is texture ratio.

For all the separated gray level components, the derivation of co-occurrence matrices, $\mathbf{P}_{\theta,d}(i,j)$ were done for different directions. For all pixels (i_1,j_1) in the image, there are (i_2,j_2) at a distance, d in direction, θ were determined. In this section, texture features were quantified as mean, variance, standard deviation, range, contrast, energy, homogeneity, correlation and entropy. The corresponding procedure is given in equation (3) through (11).

$$\mu = \sum_{i=1}^{n} \mu_i \sum_{j=1}^{n} \mu_j \tag{3}$$

$$Var = \sum_{i=0}^{n} (i-\mu_i)^2 \mathbf{p}(i,j) \sum_{j=0}^{n} \left(j-\mu_j\right)^2 \mathbf{p}(i,j) \tag{4}$$

$$SD = \sqrt{\text{Var}} \tag{5}$$

$$R = \max.[\mathbf{p}(i,j)] - \min.[\mathbf{p}(i,j)] \tag{6}$$

$$CON = \sum_{i,j=0}^{n-1} (i-j)^2 \, \mathbf{p}(i,j) \tag{7}$$

$$EG = \sum_{i=0}^{n-1} \sum_{j=0}^{n-1} \mathbf{p}^2(i,j) \tag{8}$$

$$HOM = \sum_{i,j=0}^{n-1} \frac{\mathbf{P}((i,j)}{1+|i-j|} \tag{9}$$

$$CO = \sum_{i=0}^{n-1} \sum_{j=0}^{n-1} \frac{(i-\mu_i)(j-\mu_j)}{\sigma_i \sigma_j} \mathbf{P}(i,j) \tag{10}$$

$$EN = \sum_{i=0}^{n-1} \sum_{j=0}^{n-1} \mathbf{P}(i,j) \log_2 \mathbf{p}(i,j) \tag{11}$$

where $\mathbf{p}(i,j)$ – gray level co-occurrence matrix, μ – mean, *SD* – standard deviation, *Var* – variance, *R* – range, *CON* – contrast, *EG* – energy, *HOM* – homogeneity, *CO* – correlation, and *EN* – entropy.

TEXTURE FEATURE REPRESENTATION

Once the features were extracted, the next step was to find to which class does the query image belong. In this section, the nine texture features that were extracted were used as input vectors. As indicated in Figure 2, the output vectors (classes) were represented by using binary numbers, 0 and 1.

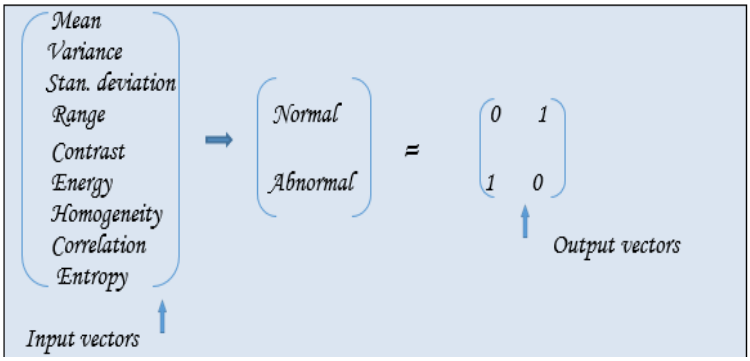

Fig. 2. Vector representation of texture features.

Since we had two classes that correspond to the normal and abnormal tissue image, we used two binary numbers, 0 and 1. If the value of the column vector is 0, it indicates that the feature data set is the member of the normal class; if it is 1, it indicates that the feature data set is the member of abnormal liver class.

CLASSIFICATION OF LIVER IMAGES

In this work, the classification of liver images was performed by a neural network classifier. It requires a set of training data and another set of testing data to train and evaluate the performance of the classifier. The sample data for training liver images were obtained from a radiologist who has assigned labels to a set of normal and abnormal images.

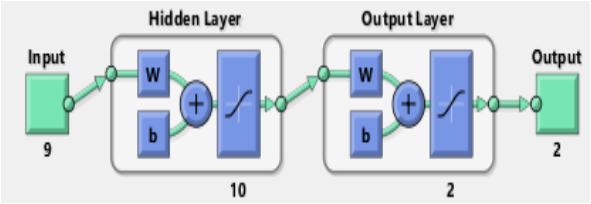

Fig. 3. Network diagram of texture features.

The nine texture features were selected as input to the network. Accordingly, the network was designed to have nine input layers, ten hidden layers and two output layers.

LIVER TUMOR SEGMENTATION

Liver tumor was segmented using Otsu thresholding due to its simplicity and the difference in the gray levels intensities, which calculates different threshold for different images based on within classes and between classes variance. The algorithm works based on pixel distributions and similarity among the pixels within a region.

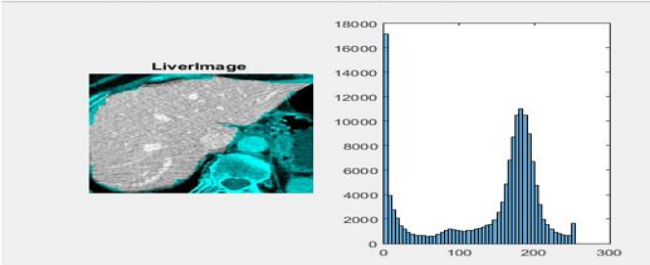

Fig. 4. Histogram of the liver image.

The histogram shown in Figure 4 is suitable for image thresholding. The bottom-right region of the image contains the tumor. A histogram of the image is analyzed and the highest pitch represents the middle intensity of tumor region. The valley point is usually chosen as the threshold. In bi-level thresholding, all the gray level values greater than the threshold values were assigned the "tumor" label and all the other gray level values were assigned the "background" label. Thus, the tumor pixels were separated from the background pixels.

$$g(x,y) = \begin{matrix} 1, & \text{for } f(x,y) \geq T \\ 0, & \text{for } f(x,y) < T \end{matrix} \tag{12}$$

where, T is the threshold value, $g(x,y)$ is the pixel of tumor, $f(x,y)$ is the pixel of values of the liver image. Then, after thresholding, the area opening technique was used to remove the connected components from a binary image that have pixels lower than a set of value based on the procedures suggested by Al Mahmud *et al.* [1]. Finally, the pixel subtraction operator was applied, which takes two images as input and produces a third image as an output by simply operating the difference in pixel values of the given images [4].

$$Q(i,j) = R(i,j) + S(i,j) \tag{13}$$

where *Q*, *R*, and *S* represent the output image, the thresholding image and the opened image, respectively.

MORPHOLOGICAL FEATURE REPRESENTATION

Once the features were extracted, the next step was to find to which class does the query image belong. In this section, the six morphological features that were extracted, were used as input vectors. As indicated in Figure 5, the output vectors (classes) were represented by using binary numbers, 0 and 1.

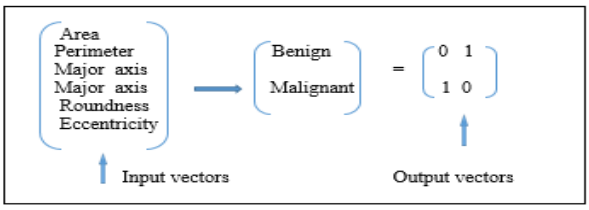

Fig. 5. Vector representation of morphological features.

If the value of the column vector is 0, it indicates that the feature data set is the member of the benign class and if it is 1, it indicates that the feature data set is the member of malignant class.

TUMOR CLASSIFICATION

Tumor classification was carried out by the morphology of binary image using a neural network classifier. The sample data for training were CT images obtained from a radiologist, who has assigned labels to a set of benign and malignant liver tumors. The six morphological features were used as input to the network. Accordingly, it was designed to have six input layers, ten hidden layers and two output layers.

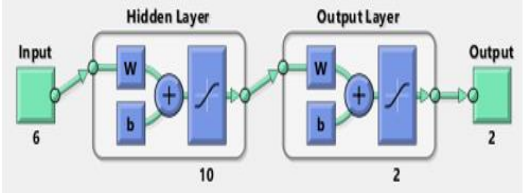

Fig. 6. Network diagram of morphological features.

Classification accuracy was characterized by the mean squared error (MSE) and percent error (% *E*). If the results of MSE and % *E* are small in the samples given for training, testing and validation, the value is observed in either confusion matrix or ROC curve. In this work, we only used the confusion matrix (Table 1).

Table 1
Confusion matrix

	Positive	**Negative**
Positive	*TP*	*FP*
Negative	*FN*	*TN*

Here, *TP* represents the mass lesion marked as malignant, which is also classified as malignant; *TN* represents mass lesion marked as benign, which is also classified as benign; *FP* represents mass lesion marked as malignant, but classified as benign; *FN* represents the mass lesion marked as benign, but classified as malignant. The mathematical equations used to evaluate the performance of the classifier for tumor classification were the following:.

$$Sensitivity = \frac{TP}{TP+FN} \tag{14}$$

$$Specificity = \frac{TN}{TN+FP} \tag{15}$$

$$Accuracy = \frac{TP+TN}{TN+TP+FP+FN} \tag{16}$$

RESULTS

In this section, the results of detection, extraction and classifications of liver and tumors are presented.

PRE-PROCESSING RESULTS

The eroded image shown in Figure 7a was obtained by an erosion technique having ‘diamond’ structure element with ‘radius’ of 2, which removes undesirable information from the original CT image. Then, it undertakes a median filtering to increase its enhancement, as shown in Figure 7b. The enhancement was performed with a median operator of kernel of 5×5 pixels by going through each pixel of the original image and replacing the value of the pixel in question by the median of its neighboring pixels.

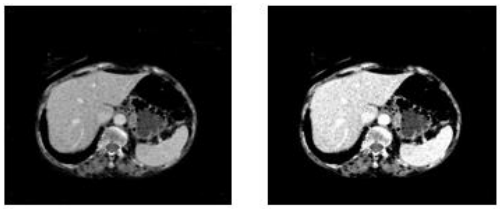

a) b)
Fig. 7. Pre-processed CT image: a) eroded image, b) enhanced image.

LIVER SEGMENTATION RESULTS

The steps conducted for the segmentationof normal and abnormal liver images are shown in Figure 8. They were performed in a semi-automatic manner, which created a binary mask from the liver with all pixel values of the liver to 1 and all pixel values outside the ROI to 0. Finally, the liver was delineated from other parts of the CT image using the green component of the RGB image.

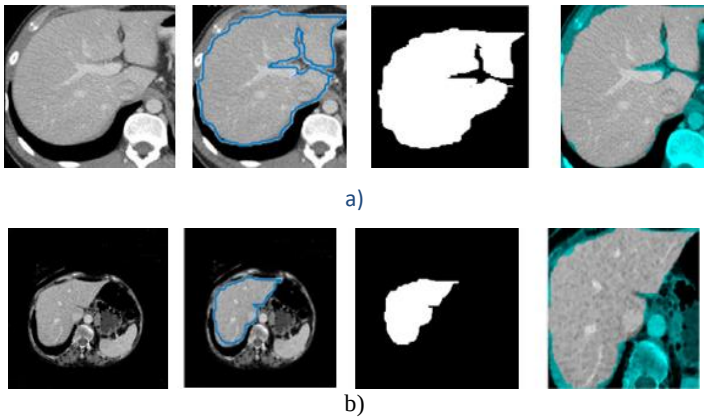

a)

b)

Fig. 8. Segmentation of liver images: a) normal liver, b) abnormal liver.

TEXTURE BASED LIVER CLASSIFICATION RESULTS

The result of texture feature extraction of liver images shown in Table 2.

Table 2
Texture features sample

Texture features									
Liver images	Mean (pixel)	Variance (pixel)	Standard deviation (pixel)	Range (pixel)	Contrast	Energy	Homogeneity	Correlation	Entropy (Bit per pixel)
Normal	1020	1.1869e+07	3.445e+03	2768	0.03	0.25	0.98	0.99	1.30
Abnormal	1029	1.2704e+07	4.015e+03	2304	0.16	0.19	0.62	0.68	1.18

As shown in Table 2, abnormal liver images had lower energy, homogeneity, correlation and entropy and higher contrast than normal liver images. This indicates that there are some variation in neighboring pixel values in the gray level of abnormal liver images compared to normal ones. As a result, the texture of abnormal liver images became irregular and blurred in appearance.

TUMOR SEGMENTATION RESULTS

After applying histogram based thresholding using Otsu method to the filtered gray scale image, the threshold value turned gray scale image into a binary image and the tumor edge was correctly separated from other parts of the liver image which is shown below in Figure 9.

Fig. 9. Detection of liver tumor.

The steps for tumor segmentation using different techniques with different steps tested through different types of images are shown in Figure 10.

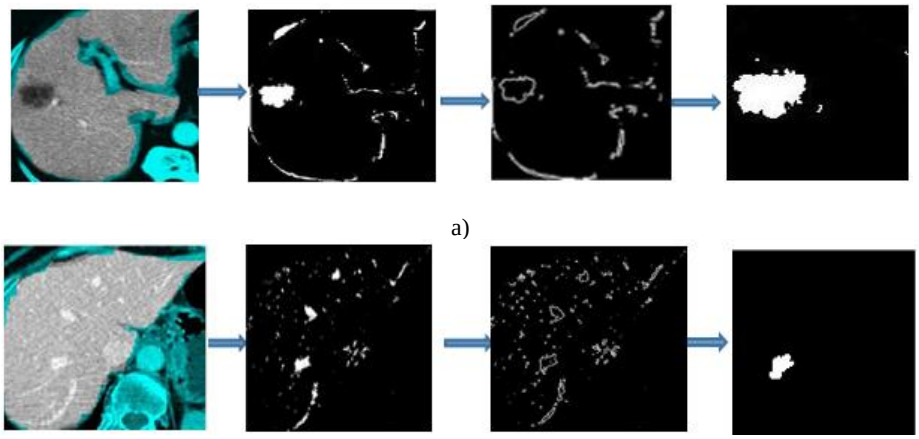

a)

b)

Fig. 10. Liver tumor segmentation: a) benign tumor, b) malignant tumor.

As shown in Figure 10, first the liver image was enhanced by removing the noise via median filtering and converted to binary image using the thresholding technique. Then, the area opening technique was used to clean the image by eliminating components of lower pixel values than a preset value. Finally, the tumor was segmented by subtracting the clean image from the binarized one using the image subtraction operator.

MORPHOLOGICAL EXTRACTION RESULTS

The results of morphological feature extraction of liver tumors are listed in Table 3.

Table 3

Results of morphological feature extraction

Morphological features						
Liver tumors	**Area (mm^2)**	**Perimeter (mm)**	**Major axis (mm)**	**Minor axis (mm)**	**Eccentricity**	**Roundness**
Malignant	1320	63.44	17.48	12.04	0.47	0.50
Benign	716	76.32	15.47	9.31	0.75	0.85

From the selected sample of malignant and benign liver tumors shown in Table 3, benign liver tumors had circular shape or more rounded and eccentric geometry than malignant liver tumors.

TUMOR CLASSIFICATION RESULTS

Tumor classification results using morphological features are shown in Table 4.

Table 4

Confusion matrix using morphological features

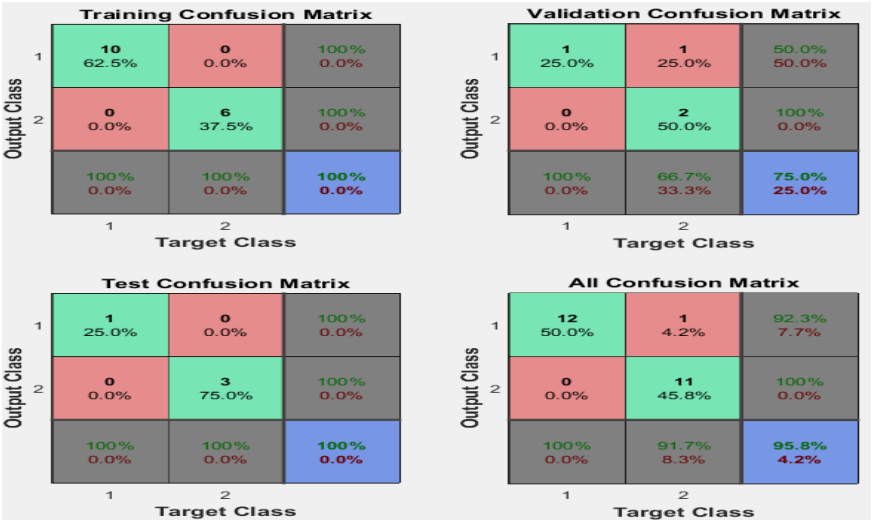

Table 4 presents the summary of the classification results produced by the ANN classifier. Using morphological features, for the total training of 16 samples (10 malignant and 6 benign) used for training, in all instances the features were correctly

classified. For the total validation of 4 samples (2 malignant and 2 benign) used for validation, 3 images were correctly classified while 1 image was misclassified. For the 4 samples (1 malignant and 3 benign) used for testing, the features were correctly classified. Finally, for the entire sample of 24 images (12 malignant and 12 benign) unseen images used for testing, 23 images (95.8 %) were correctly classified and 1 image (4.2) was misclassified.

PERFORMANCE OF THE CLASSIFIER

The classifier performance results are shown in Table 5.

Table 5

Performance results of the classifier

	TP	***FN***	***TN***	***FP***	**Sensitivity**	**Specificity**	**Accuracy**
Training	10	0	6	0	100 %	100 %	100 %
Validation	1	0	2	1	100 %	66.7 %	75 %
Test	1	0	3	0	100 %	100 %	100 %
All	12	0	11	1	100 %	91.7 %	95.8 %

DISCUSSION

The image processing techniques developed in this work were implemented to classify liver tumor using ANN. Our system consists of preprocessing techniques such as erosion and median filter where the liver images were smoothed and the edges were defined as well as the intensity of the images was increased. After image enhancement, the segmentation of the liver tumor in an image takes place. For this purpose, Otsu's thresholding was used to divide image into foreground and background regions where the tumor is in the foreground part. Then after segmentation, the tumors are classified according to their classes by using an ANN classifier.

Mittal *et al*. [11] proposed a CAD system to assist radiologists in identifying focal liver lesion in B-mode US images. Their system can be used to discriminate focal liver disease such as cyst, hemangioma and HCC and metastases along with normal liver tissue. The study used with 111 real US images comprising of 65 typical and 46 atypical images, which were taken from 88 subjects. These images were first enhanced and then ROIs were segmented into 800 non-overlapping segmented ROIs. Subsequently 208 texture based features were extracted from each segmented ROI. A two-step NN classifier was designed for classification of five liver image categories. In the 1st step the NN classifier gives classification among five liver image categories. If NN decision was for more than one class as obtained from the 1st step, binary NN classifier were used in the 2nd step for crisp classification between two classes. Test

results of two step NN classifier showed correct decisions in 432 out of 500 segmented ROIs with classification accuracy of 86.4 %. The classifier has given correct diagnosis of 90.3 % (308/340) in the tested segmented ROI from typical class and 77.5 % (120/160) in test segmented ROI from atypical cases. According to the results reported here, the newly developed CAD system outperforms the algorithm of Mittal *et al*. [11] in classifying liver tumors.

CONCLUSIONS

Tumor classification is an essential task in computer aided and automated liver cancer detection.

In this research, an artificial neural network was proposed for tumor classification. The performance of the classfier was evaluated using 36 images containing 12 normal and 24 abnormal liver of which 12 benign and 12 malignant tumors classified. The maximum accuracy rate for tumor classification is 95.8 %.

To date, different classifiers were used to analyze medical images. The ANN procedure proposed in this paper shows very good performance in comparison with other medical diagnostic systems. However, the performance of our classifier could be improved by increasing the number of training images.

Declaration: The authors declare no competing interests.

Ethical consideration: Written ethical clearance letters and wavier of informed consent were obtained from the research and ethics committee of Addis Ababa University, College of Health Sciences, Department of Radiology, Tikur Anbessa Specialized Hospital.

Acknowledgement: The authors would like to thank Radiology Department, who gave us sample of abdominal CT images in Tikur Anbessa Specialized Hospital, Addis Ababa, Ethiopia.

REFERENCES

1. AL MAHMUD, A., Z. KARIM, M. RAHMAN, Brain tumor detection using MR images through pixel based methodology, *Global Journal of Computer Science and Technology*, 2015, **15**(4), 302–315.
2. BAAZAOUI, A., W. BARHOUMI, A. AHMAD, E. ZAGROUBA, Semi-automated segmentation of single and multiple tumors in liver CT images using entropy-based fuzzy region growing, *IRBM*, 2017, **38**(2), 98–108.
3. CLARK, H.P., W.F. CARSON, P.V. KAVANAGH, C.P. HO, P. SHEN, R.J. ZAGORIA, Staging and current treatment of hepatocellular carcinoma, *Radiographics*, 2005, **25**, Suppl 1, S3-23, DOI: 10.1148/rg.25si055507.
4. GONZALEZ, R.C., R.E. WOODS, S.L. EDDINS, *Digital Image Processing Using Matlab*, 2nd edition., Gatesmark Publishing, LLC, 2009.
5. HARALICK, R., K. SHANMUGAM, I.H. DINSTEIN, Textural features for image classification, *IEEE Transactions on Systems*, 1973, **3**, 610–621.

6. HOPPER, K.D., K. SINGAPURI, A. FINKEL, Body CT and oncologic imaging, *Radiology*, 2000, **215**, 27–40.
7. LEONDES, C.T. (ed.), *Medical Imaging System Technology: Analysis and Computational Methods*, World Scientific Publishing Company, New Jersey, London, Singapore, 2005, pp. 363–386.
8. MALIK, J., S. BELONGIE, J. SHI, T. LEUNG, Textons contours and regions: Cue integration in image segmentation, *Proc. IEEE Intl. Conf. Computer Vision*, Corfu, 1999, **2**, 918–925.
9. MASUTANI, Y., K. UOZUMI, A. MASAAKI, O. KUNI, Liver CT image processing: A short introduction of the technical elements, *European Journal of Radiology*, 2006, **58**, 246 –251.
10. MEKONNEN , D., A. DERBIE, F. BIADGLEGNE, *et al*., Knowledge and practice on magnitude, diagnosis, treatment and prevention strategies of hepatocellular carcinoma in Ethiopia: A systematic review chronic liver cancer report, *The Ethiopian Journal of Health Development*, Addis Ababa, Ethiopia, 2017, **31**(1), 44–56.
11. MITTAL, D., V. KUMAR, S.C. SAXENA, N. KHANDELWAL, N. KALRA, Enhancement of the ultrasound images by modified anisotropic diffusion method, *Med. Biol. Eng. Comput.*, 2010, 48, 1281–1291.
12. RIKABI, A., A. BENER, A. AL-MARRI, S. AL-THANI, Hepatitis B and C viral infections in chronic liver disease: A population-based study in Qatar, *Eastern Mediterranean Health J.*, 2009, **15**(4), 778–784.
13. SAHOO, P.K., S. SOLITANI, A.K.C. WONG, Y.C. CHEN, A survey of thresholding techniques, *Comput. Vision Graph. Image Process*., 1988, **41**, 233–260.
14. SHANNON, C.E., Communication in the presence of noise, *Proceedings of the Institute of Radio Engineers*, 1949, **37**, 10-21, https://doi.org/10.1109/JRPROC.1949.232969.
15. SINHA, T., Tumors: benign and malignant, *Canc.Therapy and Oncol. Int. J*., 2018, **10**(3), 52–54.